Development of a standardized in vitro approach to evaluate microphysical, chemical, and toxicological properties of combustion-derived fine and ultrafine particles

Ana Teresa Juarez-Facio, Clément Castilla, Cécile Corbière, Hélène Lavanant, Carlos Afonso, Christophe Morin, Nadine Merlet-Machour, Laurence Chevalier, Jean-Marie Vaugeois, Jérôme Yon, et al.

Development of a standardized *in vitro* approach to evaluate microphysical, chemical, and toxicological properties of combustion-derived fine and ultrafine particles

Ana Teresa Juarez-Facio[1], Clément Castilla[2], Cécile Corbière[1], Hélène Lavanant[2], Carlos Afonso[2], Christophe Morin[2], Nadine Merlet-Machour[2], Laurence Chevalier[3], Jean-Marie Vaugeois[1], Jérôme Yon[4], Christelle Monteil[1*]

1. Normandie Univ, UNIROUEN, UNICAEN ABTE, 76000 Rouen, France
2. Normandie Univ, UNIROUEN, INSA Rouen, CNRS, COBRA, 76000 Rouen, France
3. Normandie Univ, UNIROUEN, INSA Rouen, CNRS, GPM-UMR6634, 76000 Rouen, France
4. Normandie Univ, UNIROUEN, INSA Rouen, CNRS, CORIA, 76000 Rouen, France

Abstract: Ultrafine particles represent a growing concern in the public health community but their precise role in many illnesses is still unknown. This lack of knowledge is related to the experimental difficulty in linking their biological effects to their multiple properties, which are important determinants of toxicity. Our aim is to propose an interdisciplinary approach to study fine (FP) and ultrafine (UFP) particles, generated in a controlled manner using a miniCAST (Combustion Aerosol Standard) soot generator used with two different operating conditions (CAST1 and CAST3). The chemical characterization was performed by an untargeted analysis using ultra-high resolution mass spectrometry. In conjunction with this approach, subsequent analysis by gas chromatography–mass spectrometry (GC-MS) was performed to identify polycyclic aromatic hydrocarbons (PAH). CAST1 enabled the generation of FP with a predominance of small PAH molecules, and CAST3 enabled the generation of UFP, which presented higher numbers of carbon atoms corresponding to larger PAH molecules. Healthy normal human bronchial epithelial (NHBE) cells differentiated at the air-liquid interface (ALI) were directly exposed to these freshly emitted FP and UFP. Expression of *MUC5AC*, *FOXJ1*, *OCLN* and *ZOI* as well as microscopic observation confirmed the ciliated pseudostratified epithelial phenotype. Study of the mass deposition efficiency revealed a difference between the two operating conditions, probably due to the morphological differences between the two categories of particles. We demonstrated that only NHBE cells exposed to CAST3 particles induced upregulation in the gene expression of *IL-8* and *NQO1*. This approach offers new perspectives to study FP and UFP with stable and controlled properties.

Keywords:
In vitro
Air-Liquid Interface
miniCAST
fine and ultrafine particles
organic compounds
OC/TC

---

* Corresponding author. E-mail: christelle.monteil@univ-rouen.fr (C. Monteil).

Introduction

Air pollution is a serious worldwide issue due to its health impacts. As classified by the International Agency of Research on Cancer (IARC) as carcinogenic to humans (Group 1), air pollution led to 8.8 million early deaths in 2015 (Lelieveld et al., 2019). The strongest evidence for public health concerns mostly includes coarse (PM_{10}, i.e. PM with a median aerodynamic diameter <10 µm) and fine particulates (FP, $PM_{2.5}$, i.e. PM with a median aerodynamic diameter <2.5 µm). This has been demonstrated both after short- and long-term exposures for cardiovascular and respiratory diseases, as well as for all-cause mortality (Brook et al., 2010; Burnett et al., 2018; Pope et al., 1995).

There is a growing concern in the scientific community about the contribution of ultrafine particles (UFP, PM with a median aerodynamic diameter of 100 nm or less; $PM_{0.1}$) to human health. Indeed, physical factors such as size and morphology participate in the toxicity of particles by letting them penetrate into the different regions of the respiratory system (Carvalho et al., 2011; Tyler et al., 2016). Depending on its size, PM is deposited in different parts of the respiratory system: PM_{10} in upper airways, $PM_{2.5}$ in the lower airways including alveoli (Nemmar et al., 2013) and UFP, which can be translocated to interstitial sites in the respiratory tract and in extrapulmonary organs (Kreyling et al., 2009; Oberdörster et al., 2004). The large surface area of UFP enables them to deliver a greater quantity of chemical compounds to the respiratory system for a given mass of PM, playing an important role in their toxicological effects (Abdel-Shafy and Mansour, 2016; Chen and Lippmann, 2009; Tyler et al., 2016). Several studies have demonstrated the role played by PM in the oxidative stress and inflammation response (Donaldson et al., 2002; Leikauf et al., 2020; Li et al., 2003; Nemmar et al., 2013; Schraufnagel, 2020). However, despite their higher number and

important reactivity, UFP have been less studied than coarse and FP (Schmid et al., 2009). Total PM emissions include both filterable PM, directly emitted from the source as solid or nonvolatile liquid particles, and condensable PM, initially in the vapor phase after combustion and immediately forming solid or liquid droplets. Both these condensable and filterable PM form UFP (Feng et al., 2018; Kwon et al., 2020). Another characteristic of the UFP are their very short atmospheric lifetimes: their concentrations decrease with increasing distance from the emission sources (Zhang et al. 2014), hence efficient sampling strategies to collect sufficient PM mass are required (Kumar et al., 2021). An alternative is to conduct experiments with a source providing relevant emissions of UFP that can be easily produced in a reproducible way.

The mini-Combustion Aerosol Standard (mini-CAST) is a reference soot generator in which soot particles, produced from a co-flow propane diffusion flame, are quenched and quickly diluted to stabilize the soot particle stream and prevent water condensation. Many studies have been carried out to analyze the properties of soot particles, demonstrating that soot particle characteristics (such as Organic Carbon (OC) / Total Carbon (TC), morphology, number and size distribution) can be varied depending on the operating conditions, while maintaining a stable and repeatable source (Bescond et al., 2016; Jing, 1999; Moallemi et al., 2019; Moore et al., 2014). The mini-CAST has been used primarily as a calibration device for soot and to understand soot formation and has been adapted for liquid fuels. Recently, it has been used as a relevant tool in the production of aircraft soot analogues (Marhaba et al., 2019). Thus, the miniCAST soot generator should serve as an adequate device for studying particle toxicity with microphysical and chemical properties representative of real-world emissions.

The toxicity of inhaled airborne particles can be studied by different *in vivo* and *in vitro* techniques. Concerning the *in vitro* approaches, submerged assessments are commonly chosen, where cells are exposed to a particle suspension, but these are not representative of physiological conditions (Loret et al., 2016). Conversely, particle exposure of lung cells grown at the air-liquid interface (ALI) depicts a situation close to physiological conditions and allows estimation of the toxicity of combustion particles (BéruBé et al., 2010; Bhowmick and Gappa-Fahlenkamp, 2016; Paur et al., 2011). Here, cells were cultured on the semi-permeable membranes of a trans-well insert in a culture well where medium was supplied only from the basal pole. Then cells were exposed to an aerosol at the apical pole. Several devices have been developed in order to study this approach, such as the Cultex® System and the Vitrocell ® System (Aufderheide and Mohr, 2004, 2000). Despite the advantages provided by these devices, controlled and repeatable cell exposures at relevant airborne

concentrations are scarce. However, these devices, associated with the use of novel tissue engineering tools, are attractive tools to extend the knowledge on the cellular effects of UFP. Among these novel cellular tools, normal human bronchial epithelial (NHBE) cells can differentiate into a mucociliary phenotype similar to *in vivo* conditions. Additionally, when cultured at the air-liquid interface, NHBE cells are adapted to direct aerosol exposure, allowing preservation of the physical and chemical characteristics of the aerosol (Bhowmick and Gappa-Fahlenkamp, 2016; Zavala et al., 2020).

Several experimental *in vitro* studies at the ALI have demonstrated the role of oxidative stress and inflammation in FP- and UFP-induced respiratory toxicity (Crobeddu et al., 2017; Diabaté et al., 2008; Sotty et al., 2019). These effects may be due to the organic composition and polycyclic aromatic hydrocarbon (PAH) contents (Akhtar et al., 2014; Li et al., 2003), although other studies suggest that the relationship between biological response and chemical composition is much more complex (Schwarze et al., 2007). Indeed, in the study of Schwarze et al. (2007), the authors outlined the importance of size and composition, which may lead to different cellular responses. The issue of what characteristics make a particle more biologically reactive than others is pivotal, but needs further investigation and the development of suitable experimental tools.

This work aims to propose an integrated approach suitable for the physical, chemical, and toxicological characterization of FP and UFP. For that, a miniCAST soot generator was used under two different operating conditions (CAST1 and CAST3) generating particles made respectively of low and high OC/TC. First, we examined the microphysical properties of these particles as well as their deposition efficiency using an ALI device. Then, we characterized their chemical properties by a non-targeted approach using ultra-high resolution mass spectrometry and a direct insertion probe (DIP FTICR-MS), and a targeted approach using GC-MS. Finally, we conducted *in vitro* toxicity assays using the ALI-differentiated model of NHBE.

1. Materials and methods

1.1 Experimental setup

The exposure system is comprised of several main components: soot generator miniCAST (5201c, Jing Ltd., Switzerland), the Vitrocell® exposure system (model VITROCELL® 6/4 CF, Vitrocell® Systems GmbH, Germany), and several devices for the physical characterization and control of aerosol generation, as described below. A schematic of the experimental setup is shown in **Fig. 1**.

Soot particles were produced with a miniCAST soot generator allowing the production of a stable and repeatable aerosol of soot particles whose size distribution, morphology, chemical composition (organic compound content) and microstructure (arrangement of graphitic planes) are variable, through modification of the propane and air flow rates. Two operating conditions (CAST1 and CAST3) were chosen for their different contents of organic carbon (Bescond et al., 2016). They are defined by four flow rates: propane (mL/min), nitrogen (L/min), oxidation air (L/min) and dilution air (L/min). The flow rates for the operating conditions studied in the present investigation are presented in **Table 1**. Aerosol from the miniCAST is delivered to the exposure system by the distribution/dilution column.

The Vitrocell® exposure system comprises two stainless steel modules (exposure module and air control module). Aerosols are delivered to the modules in parallel: the first module receiving the aerosol and the second module receiving filtered clean air as negative control. The modules are designed for simultaneous exposure of three independent replicates. The exposure module is equipped with electrodes for high voltage charging to increase particle deposition, and in addition one well contains a quartz crystal microbalance sensor system (QCM) to determine particle dose by the Vitrocell® software. Since the QCM is not equipped with the electrode, it was not possible to measure particle deposition efficiency when the electrostatic field was used.

Prior to exposure, the exposure wells are filled with medium and heated at 37°C by a circulating water bath. The aerosol distribution to the different wells is ensured by four isokinetic sampling ports. Finally, for each well, exposure is ensured by a designed trumpet pipe, which enables the aerosol to pass over the apical pole of the cell layer (placed on the adaptors for 12-well sized inserts) at a flow rate of 10 mL/(min·well) driven by an external vacuum pump. Cells were exposed to aerosol for 35 min and control samples were exposed for 35 min to ambient HEPA-filtered laboratory air through the Vitrocell System. An electrostatic field (+1000 V) was applied to increase the rate of particle deposition.

The distribution/dilution column includes a sampling point that is connected to the dilution system (Palas VKL, Palas GmbH, Germany) for complementary analysis, such as the aerosol control concentration with the Pegasor Particle Sensor (PPS) (Mi3, Pegasor, Finland) or distribution size analysis with the Scanning Mobility Particle Size (SMPS-3080, TSI, USA). The total sampling flow rate of the exposure system is 12.3 L/min driven by a vacuum pump at the end of the line (flow rate from Vitrocell® system and VKL dilutors).

1.2 Particle characterization: size, mass, and morphology

The number and particle size distributions were measured with the SMPS in the range of 14.46–679.25 nm immediately downstream of the Vitrocell® system after going through the VKL dilutors. This enabled characterization of the particle number concentration at the time of deposition. The SMPS was operated at a sample flow of 0.3 L/min. SMPS data were corrected for the PALAS VKL dilutors (100). The mass concentration of the aerosol was measured with the Tapered Element Oscillating Microbalance (TEOM) (1105 Rupprecht & Patashnick Co., Inc., USA) and controlled over time with the PPS directly after the VKL dilutors. The soot particles were deposited onto a grid (200-mesh copper grid with a Formvar/carbon film, Agar Scientific) through impaction/interception (Ouf et al., 2010), and then observed by transmission electron microscopy (TEM) with a high-resolution microscope (JEM-2010 model, JEOL, Japan).

1.3 Determination of deposition efficiency

The deposition efficiency is defined here as the percentage of the aerosol mass transported by the aerosol flow exposed to the cells, which deposits on their surface. The deposition mechanisms are complex, and due to the small exposure flowrate (10 mL/min), only a fraction of the particles is deposited. This fraction was determined by combining the deposited mass rate measurement (quartz crystal microbalance QCM (Vitrocell®) integrated in the exposure module) and the mass concentration of the exposed aerosol (TEOM measurement). The increase in deposition efficiency induced by the electrostatic precipitator was evaluated by comparing the size distribution upstream and downstream of the exposure modules with the SMPS, with and without electric field.

1.4 Chemical characterization

***Non-targeted analyses*.** The non-targeted analysis of the two CAST conditions was performed using a direct insertion probe with atmospheric pressure chemical ionization source (DIP APCI) coupled to ultra-high resolution mass spectrometry (FTICR MS) (12T SolariX XR FTICR, Bruker Daltonics, USA). Cellulose filters containing particulate matter were obtained from the miniCAST exhaust next the dilution column after 35 min of cell exposure. Soot particles were scraped from the frozen filters for direct solid analysis. About 0.1 to 0.5 mg of soot particles was put in the hollow part of a glass capillary, sealed with a piece of quartz fiber filter then inserted in the DIP APCI FTICR MS system for acquisition. The amount of soot particles could not be measured more precisely because of difficulties in handling the

capillary on the precision weighing scale. Three analytical replicates were acquired for each condition, in random order to avoid systematic bias from the measurement devices.

External calibration was performed using a polycyclic aromatic hydrocarbon (PAH) mixture (Supelco EPA 610, Sigma Aldrich, France). Generally, errors below 250 ppb were found. After calibration, each individual scan of the time-resolved data was peak-picked (S/N 9) and exported with Bruker Data Analysis (5.0) visual basic scripts. The exported mass spectra were processed by self-written MATLAB routines, and molecular assignment was performed using the following restrictions: $C_cH_hN_nO_o$; $n \leq 1$ and $o \leq 4$, with a maximum error of 2 ppm, DBE≤80, 0 ≤ H/C ratio ≤ 3. The molecular formula attribution lists of the six data sets were merged into one list. All attributions were considered, and attributions not found within a sample were set to zero intensity. To ensure that the program and results were reliable, we checked whether the resulting errors calculated from the difference between experimental *m*/*z* values and *m*/*z* values predicted for the molecular formulas produced the normal distribution expected for random errors. The elemental composition attributions of the average spectra were compared via multivariate data analysis. Principal Component Analyses (PCA) were performed. Data were subjected to power transformation before PCA, to reduce heteroscedasticity and to do pseudo-scaling. The resulting scores and loadings data, combined with the elemental composition attribution, were used for visualization. In this respect, score data are linked to the experiments (replicates and sample type) and loadings data to the individual elemental compositions (molecular profile).

Targeted analyses. Aerosols were sampled on a quartz filter for 1 min in the sampling point after the miniCAST (**Fig. 1**). After collection, the filters were cut using a punch in order to obtain similar samples of 16 mm^2 surfaces. The obtained samples were introduced in glass-lined non-deactivated TDU tubes (Gerstel GmbH & Co. KG, Germany).

A PAH mixture (TraceCERT, 2000 µg/mL in benzene/dichloromethane, 1/1, *V/V*) containing 16 US EPA priority PAH was diluted to 100 µg/mL with toluene and used as the standard stock mixture for PAH. An oxy-PAH mixture (≥98.8%, 100 µg/mL in toluene) was prepared with 9-fluorenone (9-Fluo-one), Benzo(a)fluorenone (B(a)Fluo-one), 6H-benzo(c,d)pyren-6-one (B-Pyr-one), 1,4-naphtoquinone (1,4 NaphtQ) and 9,10-anthraquinone (9,10 QanthQ). Perylene-D12 and Phenanthrene-D10 were used as internal standards. All solvents used were of HPLC grade. Standard addition was used for quantification in order to prevent matrix bias. The three levels of addition ranged from 0.5 to 5 ng (3 replicates per level). The analyses were performed by using a gas chromatograph (7890-B, Agilent

Technologies, USA) coupled to a triple quadrupole mass spectrometer (MS/MS) (7000 C, Agilent Technologies, USA). This chromatograph was equipped with an external desorption unit (TDU 2, Gerstel GmbH & Co. KG, Germany) and a programmed temperature vaporization (PTV) inlet (CIS 4, cool injection system, Gertel). The temperature for thermal desorption was initially set at 30°C, then increased at 20°C/min to 350°C (held for 10 min) with helium desorption flow at 96 mL/min by using solvent vent mode. Desorbed compounds were focused at 10°C onto a quartz wool in the glass liner (1 mm i.d.) in the cooled injection system (CIS) before their analysis by GC-MS/MS. After thermodesorption, the CIS 4 unit was programmed from 10°C (held for 0.15 min) to 350°C (held for 5 min) at 720°C/min for injecting trapped compounds in splitless mode into the GC column (column DB5-5MS, 60 m × 0.25 mm i.d. × 0.10 µm, Agilent). The GC oven was programmed at 60°C for 1.2 min, increased at 40°C to 190°C, then increased at 4°C/min to 240°C and finally at 6°C/min to 305°C (held 8.5 min). Helium was used as the carrier gas at 1.4 mL/min in constant flow mode. The temperature of the transfer line between the GC and MS spectrometer was set at 310°C. MS/MS analyses were performed in Multiple Reaction Monitoring (MRM) mode. Helium was used as the quenching gas. Its flow was set at 2.25 mL/min. Nitrogen collision gas was supplied at 1.5 mL/min. Electron ionization (EI) was used for detection (70 eV, ionizing current: 35 µA). The ion source temperature was 230°C and the temperature of quadrupoles 1 and 2 was 150°C. The resolutions of MS1 and MS2 were unit and wide, respectively. One precursor ion and two product ions (1 quantifier and 1 qualifier) were selected for each analyzed compound. Nine time segments were used to perform MS/MS analyses. These segments included 1 to 5 ions within a narrow range of retention times. Collision energies were optimized for each of the 23 analyzed compounds (21 analytes plus 2 internal standards) to maximize the signal abundance of the product ions in the analysis of standard compounds. Dwell times were also optimized for each analyzed compound.

1.5 NHBE cells cultures and exposures

Primary Normal Human Bronchial Epithelial (NHBE) cells (ATCC-PCS-300-010™, USA) were obtained from biopsies isolated from a healthy donor. NHBE cells were maintained until

confluence (75%-80%) in 75 cm^2 plastic flasks (BD Falcon ®, Corning, USA) in Airway Epithelial Cell Basal Medium (ATCC, USA) complemented with a Bronchial/Tracheal Epithelial Cell Growth Kit (ATCC, USA) supplemented with Penicillin (10 Units/mL; GIBCO USA) and Streptomycin (10 µg/mL; GIBCO, USA). Then, cells were seeded at a density of approximately 80,000 cells per cm^2 on collagen-coated 12 mm Transwell®, 0.4 µm Pore Polyester Membrane Inserts (Costar®, STEMCELL Technologies Inc., France). Once cells had reached confluence (3 days) ALI conditions were established by removing the apical medium and replacing the basal medium by Pneuma-CultTM-ALI Basal medium (STEMCELL Technologies Inc., France) complemented with Pneuma-CultTM-ALI 1X Supplement (STEMCELL Technologies Inc., France), PneumaCultTM-ALI 1X Maintenance Supplement (STEMCELL Technologies Inc., France) and hydrocortisone (2 µmol/L) (STEMCELL Technologies Inc., France). In order to determine the culture conditions to allow progressive differentiation into ciliated, globet and basal cell types within a pseudo-stratified epithelium, NHBE cells were grown until 0, 7, 14 or 21 days at ALI before gene expression of differentiation markers was performed.

Air-liquid interfaces were maintained for 14 days (prior to exposure). Mucus production was removed with a gentle saline rinse (PBS-1X, GIBCO, USA) 1 day prior to exposure. Cells were maintained in 95% humidified air with 5% CO_2 at 37°C. During exposures cells were placed in the Vitrocell ® system and exposed on-line to fresh particles (CAST1 and CAST3) for a duration of 35 min (minimum n=3 per treatment group). Control cells were exposed to the same conditions described above but to filtered air. We compared the response of particle-exposed cells with the response of control cells, 3 hr after exposure.

1.6 NHBE microscopy observations

NHBE cells were directly fixed on the Transwell®, 0.4 µm Pore Polyester Membrane Inserts in 2.5% Glutaraldehyde (EMS, USA) in 0.2 mol/L Hepes buffer pH 7.4 (VWR, USA). After several rinses in buffer, membrane inserts were removed from their support and cut in small pieces. Samples were post-fixed in 1% Osmium tetroxide (EMS, USA) for 1 hr at + 4°C and rapidly rinsed again. Cells were then dehydrated using a graded series of ethanol and acetone before being impregnated with Epoxy Low Viscosity Resin (EMS, USA) under vacuum. The resin was polymerized at 60°C between 48 to 72 hr. For optical microscopy, 800 nm-thin sections were prepared by ultramicrotomy (Ultracut-UCT, Leica-microsystems, Germany)

and stained with toluidine Blue (EMS, USA), a metachromatic dye. Observations were performed on an upright light microscope (DM6B, Leica-microsystems, Germany) and images acquired with a sCMOS camera (DFC9000, Leica-microsystems, Germany).

For transmission electron microscopy, ultrathin sections (50-70 nm, Ultracut-UCT Leica-microsystems, Germany) were collected on gold 600 mesh grids and stained 7 min with 0.5% uranyl acetate in methanol solution. Conventional TEM observations were performed on JEM 2010 operating at 120 kV and equipped with a LaB6 cathode, an SDD-detector (Oxford Instruments, UK), a CDD camera (Erlangshen 500 Gatan, USA) driven by Digital Micrograph software (Gatan-Ametek, USA). High-Resolution images were acquired on JEM-ARM200F HRTEM (JEOL Ltd., Japan) that was double-corrected, configured for analysis purposes, and equipped with an ultrascan camera (US1000, Gatan, USA) and ultrafast camera (Gatan-Ametek, USA).

1.7 Cytotoxicity and gene expression

Cytotoxicity was measured by the MTT assay 3 hr after exposure. Inserts were gently rinsed with PBS-1X. Briefly, 0.05 mL of MTT solution (50 µg/mL, Sigma Aldrich, France) in 0.5 mL of medium was added to the lower chamber (basal) for 3 hr. Then 0.5 mL of SDS (10% in 0.1 mol/L HCl) were added to the lower and upper chambers and incubated during the night to dissolve the purple crystals. The extracted solution was transferred to 96-well plates, and absorbance was measured at 570 nm using the SAFAS (Xenius, Safas, Monaco). The absorbance of the samples was normalized to the control, which was set to 100%.

For the study of gene expressions, total RNA was extracted from cells using TRI-REAGENT® (Sigma-Aldrich, France) and Direct-zol™ RNA MiniPrep (Ozyme, France). RNA concentration and purity were measured with a NanoDrop spectrophotometer (NanoDrop™ 2000 / 2000c, Thermo Fisher Scientific Inc., USA). All the RNA integrity numbers of the samples were > 8. cDNA was prepared by reverse transcribing extracted RNA samples using Invitrogen™ Transcriptase inverse M-MLV (Invitrogen, USA). The expression of mRNA was determined by the quantitative real time polymerase chain reaction (qRT-PCR) using Brilliant III Ultra-fast SYBR Green QPCR Master Mix (Agilent Technologies, USA) and Stratagene Mx3005P (Agilent Technologies, USA). Expression profiles were normalized to the housekeeping gene B2M. Only the results of qRT-PCR comprising between 80%-110% efficiency were considered. Results for differentiation genes are expressed as absolute quantification $\Delta Ct = Ct_{(\text{target gene})} - Ct_{(\text{housekeeping gene})}$, while oxidative and inflammatory genes are expressed as absolute quantification $\Delta Ct = Ct_{(\text{target gene})} - Ct_{(\text{housekeeping gene})}$ and oxidative

and inflammatory genes are expressed as relative expression (fold change) using the $2^{-\Delta\Delta Ct}$ method (Livak and Schmittgen, 2001). All primer sequences used in this work are shown in Appendix A **Table S1**.

1.8 Statistical analysis

Results were expressed as mean ± standard deviation (SD). Statistical analysis of gene expression was performed using the non-parametric Mann-Whitney U-test (GraphPad for Windows, v8.0). Statistically significant differences were reported with $p < 0.05$.

2. Results

2.1 Particle characterization: size, mass, and morphology

The particle size distribution within the aerosol can be seen in **Fig. 2** The geometric median (GM) mobility diameter, particle number, and mass concentration for each different operating condition are shown in **Table 2**. Particle emission depends on the operating conditions. CAST3 produced a smaller size distribution compared to CAST1. The mass concentration for CAST1 condition is higher (89.4 mg/m^3) compared with CAST3 (57.9 mg/m^3).

Concerning the particle morphology, the two operating conditions produced fractal aggregates, which is typical of soot particles. **Fig. 3** confirms that CAST3 produces smaller particles than CAST1. Nevertheless, the primary spheres were not very different. Indeed, according to Bescond et al. (2016), the primary sphere diameter is 26.6 nm for CAST1 and 29.9 nm for CAST3.

2.2 Particle mass deposition efficiency

Mass deposition during exposures with or without electrostatic field is shown in **Table 3.** A better deposition efficiency was observed with the CAST3 compared to the CAST1 operating condition. This discrepancy is probably due to a morphological difference between the two categories of particles, as observed in **Fig. 3,** using transmission electronic microscopy**.** The deposition efficiency was low, whatever the experimental CAST conditions (0.29% to 1.3%) but was increased with an electrostatic field (5.5 to 7.7-fold), allowing it to reach 1.78 µg·cm^2 in a 35 min exposure.

2.3 Non-targeted analyses

The two conditions CAST1 and CAST3 were compared using DIP APCI FTICR MS. One list of 1600 molecular formulas was obtained for all conditions and replicates. **Fig. 4** illustrates

the score plot for the two principal components (PC1 and PC2), which explained 99% of the total variance. PC1 explained 98% of the variation of the sample. The analytical replicates were more similar to each other for the CAST3 conditions and showed more spread for the CAST1 conditions.

Fig. 5 shows a double bond equivalent (DBE) vs carbon number plot for molecular formulas containing only hydrogen and carbon (hydrocarbons HC). DBE accounts for the amount of unsaturation present in a molecule, including double bonds or rings.

DBE vs C plots are often used for the analysis of complex samples as they can give information on the molecular structures in the sample, focusing on certain molecular classes (Marshall and Rodgers, 2008). These plots include information on the relative intensity of the observed ion, with the dot size and color coding matched to the PC loadings: red indicates a positive PC coefficient, linked to CAST1 conditions, while green is related to a negative PC coefficient more often found in CAST3 conditions.

Here, the ions from hydrocarbon compounds clearly showed two distinct families. Ions of high intensity were observed with DBE values between 5 and 25 and between 10 and 35 carbon atoms that share the characteristics of PAH, whose DBE and carbon number roughly follow the red PAH line represented in **Fig. 5**. CAST1 produced more compounds with a low number of carbons (below 15), that correspond to small PAH molecules. Conversely, CAST3 showed hydrocarbons with higher numbers of carbon atoms corresponding to larger PAH molecules. Many other low-intensity compounds with DBE values below 5 were observed with similar intensity in CAST1 and CAST3, as shown in the light orange PC1 coefficient color indicative of very small PC loadings.

From the raw molecular formulas, a putative structure was determined for each compound with the highest and lowest PC loadings (negative for CAST1 and positive for CAST3). These compounds are found in Appendix A **Tables S2** and **S3**. Low-mass PAH molecules with the lowest PC1 coefficients most likely corresponded to naphthalene, acenaphthylene, acenaphthene and anthracene (Appendix A **Table S2**). Higher mass PAH molecules with high PC loadings could correspond to pyrene, benzo(a)fluorene, benzo[ghi]fluoranthene and benzo[ghi]perylene (Appendix A **Table S3**).

2.4 Targeted analyses

The quantitative analysis tested for the 16 priority PAH and 5 oxy PAH (Appendix A **Fig. S1**). For CAST1, the low-mass PAH (2-3 aromatic rings) represented 70% of the total deposit. Acenaphthylene, fluorene and phenanthrene showed amounts higher than 10 ng/cm^2. The

other 30% were mainly represented by fluoranthene and pyrene. The total amount ranged from 200 to 400 ng/cm^2 depending on the sampling localization. For CAST3, the PAH repartition covered a larger range of aromatic cycle numbers: from 10% to 15% for low-mass PAH (2-3 aromatic rings), 40%-50% for the 4-aromatic ring PAH and 35%-40% for the heavy-mass PAH (5-6 aromatic rings). For CAST3, fluoranthene and pyrene presented amounts higher than 10 ng/cm^2. Benzo[ghi]perylene was also found at this amount. The total PAH mass ranged from 400 to 700 ng/cm^2. These results are consistent with non-targeted analyses and confirm the presence of the suggested molecules. The total amount of PAH is also consistent with the mass deposition determined: 591.8 ng/cm^2 for CAST1 and 1775 ng/cm^2 for CAST3. Moreover, the oxy-PAH amounts represented 3% for CAST1 with mainly 9-fluorenone and 9% for CAST3 with compounds like benzo(a)fluoranthene and benzopyrenenone.

2.5 Optimization of cell culture conditions

Fig. 6 shows the gene expression of four differentiation markers on NHBE cultured at the ALI for 0, 7, 14 and 21 days. Data are expressed as ΔCt. The lower the ΔCt the more the expression of this gene was induced. Results showed the highest expression of the *MUC5AC* gene, which is a marker of goblet cells, at 14 and 21 days in ALI (**Fig. 6a**). Expression of *FOX-J1* (**Fig. 6b**), a transcription factor that controls expression of ciliary genes, was present from 0 days to 21 days at ALI. Expression of *FOX-J1* remained at the same level at 14 and 21 days at ALI. Expression of *MUC5AC* and *FOX-J1* at 14 and 21 days means the reconstitution of a pseudostratified epithelium. Regarding membrane integrity, two junction markers were studied by quantifying the expression of *OCLN* and *ZO1 (*tight junctions). Constant expression of *OCLN* (**Fig. 6c**) and *ZO1* (**Fig. 6d**) was observed in all the conditions.

NHBE differentiation was confirmed by microscopic observation. **Fig. 7a** and **b** shows a cross-section of differentiated NHBE cells at 14 days under metachromatic toluidine blue coloration. Goblet cells appear light purple, basal and ciliated cells are blue-stained. **Fig. 7c-f** shows the subcellular characterization of NHBE cells: basal cells with long cytoplasmic extensions (white arrowhead) (**Fig. 7c**), goblet cells rich in mucus granules accumulated at the apical side of the cells to release their polysaccharide content in the extracellular space (white arrowhead) (**Fig. 7d**), ciliated cells well-differentiated as seen by the presence of mature motile cilia. The micrography shows basal bodies (BB), which constitute the intracytoplasmic part of the cilia and axoneme (AX) the external part, composed of membrane cilia and microtubules organized as 9+2 pairs. Close to the plasma membrane, transition fiber (TF) is

visible as a dense round structure. Residual centriolar vesicles (CV) are observed (**Fig. 7e**). Moreover, differentiated epithelium is characterized by several intercellular junctions located at the apical part of the lateral side (**Fig. 7f**). From these findings, which confirm the reconstitution of a pseudostratified phenotype, cell exposures were performed on differentiated NHBE cells at 14 days.

2.6 Cellular response

Then, differentiated NHBE at 14 days were exposed in the ALI system to CAST1 or CAST3 particles or filtered air (controls) with an electrostatic field. No cytotoxicity was observed under any of these conditions. Results are shown in **Fig. 8**.

Oxidative stress and inflammation markers (*NQO1* and *IL-8*) genes were measured in NHBE cells after exposure to CAST1 and CAST3 particles or filtered air. Results are shown in **Fig. 9**. No significant difference was observed in exposure to CAST1 particles. Nevertheless, expression of *IL-8* (2.02-fold) and *NQO1* (1.33-fold) was significantly modified 3 hr after exposure to CAST3 particles.

3. Discussion

The present results illustrate a methodological approach which allows comparing, in an original and innovative way, the physical, chemical, and toxicological properties of different fine and ultrafine particles, using a mini-CAST generator. In this study, we used two different operating conditions to obtain model particles containing either high (CAST3) or low (CAST1) organic contents, and exposed differentiated NHBE cells “on-line” at the air-liquid interface to be closer to realistic conditions.

Varying the oxidation airflow in the mini-CAST generates different operating conditions, allowing emission of particles with different physicochemical properties (Moallemi et al., 2019; Moore et al., 2014). For the studied operating conditions in this work, we found that the median particle size decreases (114.04 nm > 58.9 nm) and the number concentration increases (6.12×10^{7} #/cm^3 > 1.63×10^{8} #/cm^3) with decreasing oxidation airflow (CAST1 > CAST3). This is in accordance with previous studies by Bouvier et al. (2019). Bescond et al (2016) demonstrated that CAST1 contains a relatively low amount of organic compounds (OC/TC: 4.1%±3.5%), whereas CAST3 represents UFP with a high content of organic (OC/TC: 87%±5%) compounds (Bescond et al., 2016; Bouvier et al., 2019).

We then extend these observations by a careful chemical characterization with combined analytical approaches using DIP FTICR-MS and GC-MS with a focus on PAH, a family of

ubiquitous pollutants, which raises concern about their health effects (Marris et al., 2020). The non-targeted approach identified the detailed elemental compositions and class distributions of the compounds. The data showed similar PAH profiles for CAST1 and CAST3, with a predominance of small PAH molecules for the CAST1 contrary to CAST3 particles, which presented higher numbers of carbon atoms corresponding to larger PAH molecules. These results were consistent with the data from the targeted analysis by GC-MS, which confirmed the presence of high levels of PAH for CAST3, as fluoranthene, pyrene, b(a)pyrene, b(ghi)perylene, whereas lower molecular weight PAH such as acenaphthylene, fluorene or phenanthrene were found in CAST1. Previous studies showed that vehicle combustion represents an important source of PAH, at levels ranging between 4.5 to 11.3 mg PAH/m^3 (Lee et al., 1995) with a predominance of 2- or 3-ring PAH from diesel engines (Ravindra et al., 2008). Overall, it can be concluded that CAST1 and CAST3 particles present the properties of engine particles, in agreement with previous studies (Bescond et al., 2016; Moore et al., 2014).

The operating conditions of the mini-CAST were also found to affect the mass concentration (89.4 mg/m^3 vs. 57.9 mg/m^3, CAST1 vs. CAST3) and the deposition efficiency in the exposure chambers. We found a deposition efficiency of 0.29% for CAST1 and 1.3% for CAST3. These results suggest that deposition efficiency, and in general particle behavior, is not dependent on mass concentration, but rather is related to the chemical composition or physical characteristics such as the size of the aggregates' primary spheres. This observation highlights the influence of the physicochemical properties in the deposition of particles, which may be lost during the preparation of the particulate suspensions or organic extracts used in classical submerged cell cultures (Kaur et al., 2019). However, one potential limitation of the reduced deposition efficiency reported in this study is that it was insufficient to produce an observable cellular response. Hence, to obtain an adequate dose exposure able to induce a cellular response, an electrostatic field (+1000 V) was induced in the upper side of the exposure chamber to increase the deposition efficiency. The increase factor of the deposition efficiency was determined by measuring the size distribution upstream and downstream of the exposure chambers with the Scanning Mobility Particle Sizer (SMPS). Using an electrostatic field can increase the deposition efficiency from 5.5 to 7.7-fold, allowing it to reach 1.78 µg/cm^2 in a 35-min exposure. EF represents an attractive alternative allowing short-term exposure studies preserving cell viability or other biological markers (Bruijne et al., 2009; Frijns et al., 2017; Mülhopt et al., 2016; Ning et al., 2008; Sillanpää et al., 2008; Zavala et al., 2014).

Determination of the deposition dose in “real exposure conditions” is difficult. For example, using the Multiple-path particle dosimetry model (MPPD) (Applied Research Associates Inc., Raleigh, NC), Manojkumar et al. (2019), estimated that 24 hr exposure to real PM_1 concentrations resulted in PM deposition in the tracheobronchial region of 0.10-0.13 ng/cm^2. A similar study by Gualtieri et al. (2018) estimated, with the same *in silico* model, a PM deposition of 0.015-0.025 ng/cm^2. Hence, real dose exposures are variable, as several factors can interfere (gender, age, diseases, atmospheric conditions, aerosol characteristics). In any case, even if our dose exposure represents an exposure to important concentrations of PM, it was lower compared to the majority of UFP studies using PM suspensions (Leclercq et al., 2018; Sotty et al., 2019).

Primary Normal Human Bronchial Epithelial (NHBE) cells were used in this study because FP and UFP particles can reach lower airways. The gene expression of differentiation markers and microscopy showed that, after 14 days at the ALI, NHBE cells form a pseudostratified epithelial phenotype composed of ciliated, globet and basal cells as has already been shown (BéruBé et al., 2010; Bhowmick and Gappa-Fahlenkamp, 2016; Rayner et al., 2019; Stewart et al., 2012). Most studies concerning FP and UFP are performed in submerged conditions. This approach allows one to work “faster”, with higher exposure doses and with different kinds of particles, but it has many limitations such as changes in particle properties and difficulty in determining the correct delivery dose (Schmid and Cassee, 2017) and, above all, it is not representative of the conditions in the lung. Alternatively, in ALI exposure, aerosol is distributed directly on the cell cultures preserving the intrinsic properties of particles, and it is more representative of physiological conditions (Mülhopt et al., 2016). Therefore, differentiated NHBE at the ALI depict a situation close to physiological conditions and allow estimation of the toxicity of combustion particles in the lower airways. With these experimental conditions, we demonstrated that only NHBE cells exposed to CAST3 particles induced an upregulation of gene expression of *IL-8*, an inflammation marker and *NQO1*, an enzyme that exerts cytoprotective, antioxidant and anti-inflammatory effects in lungs (Li et al., 2004; Rubio et al., 2011, 2010). No significant difference was observed after exposure to CAST1 exhaust. This apparent discrepancy could be explained by the difference in mass deposition between these two conditions, although the levels remained close to those observed in the literature with nebulized diesel particles and the induction of *IL-8* expression (Hawley et al., 2014b). It is likely that the differences in organic composition between the two operating conditions played an important role in these biological effects (Billet et al., 2007; Borgie et al., 2015; Dergham et al., 2012). It is worth mentioning that no cytotoxic effect was

observed in our experimental conditions. This is in agreement with the study of Hawley et al. (2014a) where differentiated NHBE (21 days) were exposed to petro- or alternative biodiesel exhaust treated with or without a diesel particulate filter. Despite the lowered dose exposure of exhaust emissions (2-340 ng/cm^2), significant increases in transcripts associated with oxidative stress and PAH response were observed in all exposure groups (Hawley et al., 2014a). This response suggests that the lack of cytotoxicity at low exposure dose could be associated with a highly developed muco-ciliary phenotype for the NHBE, as previously demonstrated (BéruBé et al., 2010; Bhowmick and Gappa-Fahlenkamp, 2016; Rayner et al., 2019). It would be interesting to evaluate these responses on other cellular models such as the human bronchial epithelial cell line Beas-2B, which is the most commonly used cell line for respiratory toxicological studies with possible use at the ALI, as previously described (Stewart et al., 2012; Gualtieri et al., 2018).

4. Conclusions

In conclusion, this study presents a new methodological approach to study freshly emitted FP and UFP on differentiated bronchial cells with respect to their physicochemical properties. It outlines the necessity of a thorough characterization to control dose delivery, which depends on the physical and chemical characteristics of particles. Although further testing and optimization are still required, this approach offers new perspectives to study FP and UFP having properties similar to those emitted by real-world sources and to determine which characteristics are involved in the biological responses. In further study, the present methodological approach could be used with other cell models, such as pathological models, to offer new insights into the cell mechanism aggravated by FP and UFPs. It would be also interesting to study repeated exposure to lower doses.

Acknowledgments

This work was supported by ANSES (French Agency for Food, Environmental and Occupational Health and Safety; PUFBIO project, Grant number EST-2017-190) and co-supported by the Regional Council of Normandy and the European Union in the framework of the ERDF-ESF (CellSTEM project). Ana Teresa Juarez Facio received a PhD fellowship funded by ADEME (Agency for Ecological Transition). The authors would like to thank Cathy Logie, Violaine Martin de Lagarde and Marion Janona for their technical support.

The COBRA laboratory is financed by the Labex SynOrg (ANR-11-LABX-0029) and the European Regional Development Fund (ERDF HN0001343). Financial support from the

National Fourier transform ion cyclotron resonance network (FR 3624 CNRS) and the European Union's Horizon 2020 Research Infrastructures program (grant agreement 731077), are gratefully acknowledged.

References

Abdel-Shafy, H.I., Mansour, M.S.M., 2016. A review on polycyclic aromatic hydrocarbons: Source, environmental impact, effect on human health and remediation. Egypt. J. Pet. 25, 107–123.

Akhtar, U.S., Rastogi, N., McWhinney, R.D., Urch, B., Chow, C.-W., Evans, G.J., et al., 2014. The combined effects of physicochemical properties of size-fractionated ambient particulate matter on in vitro toxicity in human A549 lung epithelial cells. Toxicol. Rep. 1, 145–156.

Aufderheide, M., Mohr, U., 2004. A modified CULTEX® system for the direct exposure of bacteria to inhalable substances. Exp. Toxicol. Pathol. 55, 451–454.

Aufderheide, M., Mohr, U., 2000. CULTEX--an alternative technique for cultivation and exposure of cells of the respiratory tract to airborne pollutants at the air/liquid interface. Exp. Toxicol. Pathol. 52, 265–270.

BéruBé, K., Prytherch, Z., Job, C., Hughes, T., 2010. Human primary bronchial lung cell constructs: The new respiratory models. Toxicology, Highlights of the 2010 Annual Congress of The British Toxicology Society. Includes the Abstracts of the British Toxicology Society, Spring 2010 278, 311–318.

Bescond, A., Yon, J., Ouf, F.-X., Rozé, C., Coppalle, A., Parent, P., et al., 2016. Soot optical properties determined by analyzing extinction spectra in the visible near-UV: Toward an optical speciation according to constituents and structure. J. Aerosol Sci. 101, 118–132. https://doi.org/10.1016/j.jaerosci.2016.08.001

Bhowmick, R., Gappa-Fahlenkamp, H., 2016. Cells and culture systems used to model the small airway epithelium. Lung 194, 419–428.

Billet, S., Garçon, G., Dagher, Z., Verdin, A., Ledoux, F., Cazier, F., et al., 2007. Ambient particulate matter (PM2.5): Physicochemical characterization and metabolic activation of the organic fraction in human lung epithelial cells (A549). Environ. Res. 105, 212–223.

Borgie, M., Dagher, Z., Ledoux, F., Verdin, A., Cazier, F., Martin, P., et al., 2015. Comparison between ultrafine and fine particulate matter collected in Lebanon: Chemical characterization, in vitro cytotoxic effects and metabolizing enzymes gene expression in human bronchial epithelial cells. Environ. Pollut. 205, 250–260.

Bouvier, M., Yon, J., Lefevre, G., Grisch, F., 2019. A novel approach for in-situ soot size distribution measurement based on spectrally resolved light scattering. J. Quant. Spectrosc. Radiat. Transf. 225, 58–68.

Brook, R.D., Rajagopalan, S., Pope, C.A., Brook, J.R., Bhatnagar, A., Diez-Roux, A.V., et al., American heart association council on epidemiology and prevention, council on the kidney in cardiovascular disease, and council on nutrition, physical activity and metabolism, 2010. Particulate matter air pollution and cardiovascular disease: An update to the scientific statement from the American Heart Association. Circulation 121, 2331–2378.

Bruijne, K. de, Ebersviller, S., Sexton, K.G., Lake, S., Leith, D., Goodman, R., et al., 2009. Design and testing of Electrostatic Aerosol in Vitro Exposure System (EAVES): An alternative exposure system for particles. Inhal. Toxicol. 21, 91–101.

Burnett, R., Chen, H., Szyszkowicz, M., Fann, N., Hubbell, B., Pope, C.A., et al., 2018. Global estimates of mortality associated with long-term exposure to outdoor fine particulate matter. Proc. Natl. Acad. Sci. U. S. A. 115, 9592–9597.

Carvalho, T.C., Peters, J.I., Williams, R.O., 2011. Influence of particle size on regional lung deposition--what evidence is there? Int. J. Pharm. 406, 1–10.

Chen, L.C., Lippmann, M., 2009. Effects of metals within ambient air particulate matter (PM) on human health. Inhal. Toxicol. 21, 1–31.

Crobeddu, B., Aragao-Santiago, L., Bui, L.-C., Boland, S., Baeza Squiban, A., 2017. Oxidative potential of particulate matter 2.5 as predictive indicator of cellular stress. Environ. Pollut. 230, 125–133.

Dergham, M., Lepers, C., Verdin, A., Billet, S., Cazier, F., Courcot, D., et al., 2012. Prooxidant and proinflammatory potency of air pollution particulate matter (PM2.5–0.3) produced in rural, urban, or industrial surroundings in human bronchial epithelial cells (BEAS-2B). Chem. Res. Toxicol. 25, 904–919.

Diabaté, S., Mülhopt, S., Paur, H.-R., Krug, H.F., 2008. The Response of a Co-culture Lung Model to Fine and Ultrafine Particles of Incinerator Fly Ash at the Air–liquid Interface. Altern. Lab. Anim. 36, 285–298.

Donaldson, K., Brown, D., Clouter, A., Duffin, R., MacNee, W., Renwick, L., et al., 2002. The pulmonary toxicology of ultrafine particles. J. Aerosol Med. 15, 213–220.

Feng, Y., Li, Y., Cui, L., 2018. Critical review of condensable particulate matter. Fuel 224, 801–813.

Frijns, E., Verstraelen, S., Stoehr, L.C., Van Laer, J., Jacobs, A., Peters, J., et al., 2017. A novel exposure system termed NAVETTA for in vitro laminar flow electrodeposition of nanoaerosol and evaluation of immune effects in human lung reporter cells. Environ. Sci. Technol. 51, 5259–5269.

Hawley, B., L'Orange, C., Olsen, D.B., Marchese, A.J., Volckens, J., 2014a. Oxidative stress and aromatic hydrocarbon response of human bronchial epithelial cells exposed to petro- or biodiesel exhaust treated with a diesel particulate filter. Toxicol. Sci. 141, 505–514.

Hawley, B., McKenna, D., Marchese, A., Volckens, J., 2014b. Time course of bronchial cell inflammation following exposure to diesel particulate matter using a modified EAVES. Toxicol. In Vitro 28, 829–837.

Jing, L., 1999. Standard Combustion Aerosol Generator (SCAG) for Calibration Purposes 9.

Kaur, K., Jaramillo, I.C., Mohammadpour, R., Sturrock, A., Ghandehari, H., Reilly, C., et al., 2019. Effect of collection methods on combustion particle physicochemical properties and their biological response in a human macrophage-like cell line. J. Environ. Sci. Health Part A Tox. Hazard. Subst. Environ. Eng. 54, 1170–1185.

Kreyling, W.G., Semmler-Behnke, M., Seitz, J., Scymczak, W., Wenk, A., Mayer, P., et al., 2009. Size dependence of the translocation of inhaled iridium and carbon nanoparticle aggregates from the lung of rats to the blood and secondary target organs. Inhal. Toxicol. 21 Suppl 1, 55–60.

Kumar, P., Kalaiarasan, G., Porter, A.E., Pinna, A., Kłosowski, M.M., Demokritou, P., et al., 2021. An overview of methods of fine and ultrafine particle collection for physicochemical characterisation and toxicity assessments. Sci. Total Environ. 756, 143553.

Kwon, H.-S., Ryu, M.H., Carlsten, C., 2020. Ultrafine particles: unique physicochemical properties relevant to health and disease. Exp. Mol. Med. 52, 318–328.

Leclercq, B., Kluza, J., Antherieu, S., Sotty, J., Alleman, L.Y., Perdrix, E., et al., 2018. Air pollution-derived PM2.5 impairs mitochondrial function in healthy and chronic obstructive pulmonary diseased human bronchial epithelial cells. Environ. Pollut. 243, 1434–1449.

Lee, W.-J., Wang, Y.-F., Lin, T.-C., Chen, Y.-Y., Lin, W.-C., Ku, C.-C., et al., 1995. PAH characteristics in the ambient air of traffic-source. Sci. Total Environ. 159, 185–200.

Leikauf, G.D., Kim, S.-H., Jang, A.-S., 2020. Mechanisms of ultrafine particle-induced respiratory health effects. Exp. Mol. Med. 52, 329–337.

Lelieveld, J., Klingmüller, K., Pozzer, A., Pöschl, U., Fnais, M., Daiber, A., et al., 2019. Cardiovascular disease burden from ambient air pollution in Europe reassessed using novel hazard ratio functions. Eur. Heart J. 40, 1590–1596.

Li, N., Alam, J., Venkatesan, M.I., Eiguren-Fernandez, A., Schmitz, D., Stefano, E.D., et al., 2004. Nrf2 Is a key transcription factor that regulates antioxidant defense in macrophages and epithelial cells: Protecting against the proinflammatory and oxidizing effects of diesel exhaust chemicals. J. Immunol. 173, 3467–3481.

Li, N., Sioutas, C., Cho, A., Schmitz, D., Misra, C., Sempf, J., et al., 2003. Ultrafine particulate pollutants induce oxidative stress and mitochondrial damage. Environ. Health Perspect. 111, 455–460.

Livak, K.J., Schmittgen, T.D., 2001. Analysis of relative gene expression data using real-time quantitative PCR and the 2 (-Delta Delta C(T)) method. Methods 25, 402–408.

Loret, T., Peyret, E., Dubreuil, M., Aguerre-Chariol, O., Bressot, C., le Bihan, O., et al., 2016. Air-liquid interface exposure to aerosols of poorly soluble nanomaterials induces different biological activation levels compared to exposure to suspensions. Part. Fibre Toxicol. 13, 58.

Manojkumar, N., Srimuruganandam, B., Shiva Nagendra, S.M., 2019. Application of multiple-path particle dosimetry model for quantifying age specified deposition of particulate matter in human airway. Ecotoxicol. Environ. Saf. 168, 241–248.

Marhaba, I., Ferry, D., Laffon, C., Regier, T.Z., Ouf, F.-X., Parent, P., 2019. Aircraft and MiniCAST soot at the nanoscale. Combust. Flame 204, 278–289.

Marris, C.R., Kompella, S.N., Miller, M.R., Incardona, J.P., Brette, F., Hancox, J.C., et al., 2020. Polyaromatic hydrocarbons in pollution: a heart-breaking matter. J. Physiol. 598, 227–247.

Marshall, A., Rodgers, R., 2008. Petroleomics: Chemistry of the underworld. Proc. Natl. Acad. Sci. 105, 18090-5.

Moallemi, A., Kazemimanesh, M., Corbin, J.C., Thomson, K., Smallwood, G., Olfert, J.S., et al., 2019. Characterization of black carbon particles generated by a propane-fueled miniature inverted soot generator. J. Aerosol Sci. 135, 46–57.

Moore, R.H., Ziemba, L.D., Dutcher, D., Beyersdorf, A.J., Chan, K., Crumeyrolle, S., et al., 2014. Mapping the operation of the miniature combustion aerosol standard (Mini-CAST) soot generator. Aerosol Sci. Technol. 48, 467–479.

Mülhopt, S., Dilger, M., Diabaté, S., Schlager, C., Krebs, T., Zimmermann, R., et al., 2016. Toxicity testing of combustion aerosols at the air–liquid interface with a self-contained and easy-to-use exposure system. J. Aerosol Sci. 96, 38–55.

Nemmar, A., Holme, J.A., Rosas, I., Schwarze, P.E., Alfaro-Moreno, E., 2013. Recent advances in particulate matter and nanoparticle toxicology: A review of the in vivo and in vitro studies. BioMed Res. Int. 2013, 1–22.

Ning, Z., Sillanpää, M., Pakbin, P., Sioutas, C., 2008. Field evaluation of a new particle concentrator-electrostatic precipitator system for measuring chemical and toxicological properties of particulate matter. Part. Fibre Toxicol. 5, 15.

Oberdörster, G., Sharp, Z., Atudorei, V., Elder, A., Gelein, R., Kreyling, W., et al., 2004. Translocation of inhaled ultrafine particles to the brain. Inhal. Toxicol. 16, 437–445.

Ouf, F.X., Yon, J., Ausset, P., Coppalle, A., Maillé, M., 2010. Influence of sampling and storage protocol on fractal morphology of soot studied by transmission electron microscopy. Aerosol Sci. Technol. 44, 1005–1017.

Paur, H.-R., Cassee, F.R., Teeguarden, J., Fissan, H., Diabate, S., Aufderheide, M., et al., 2011. In-vitro cell exposure studies for the assessment of nanoparticle toxicity in the lung—A dialog between aerosol science and biology. J. Aerosol Sci. 42, 668–692.

Pope, C.A., Bates, D.V., Raizenne, M.E., 1995. Health effects of particulate air pollution: time for reassessment? Environ. Health Perspect. 103, 472–480.

Ravindra, K., Sokhi, R., Van Grieken, R., 2008. Atmospheric polycyclic aromatic hydrocarbons: Source attribution, emission factors and regulation. Atmos. Environ. 42, 2895–2921.

Rayner, R.E., Makena, P., Prasad, G.L., Cormet-Boyaka, E., 2019. Optimization of normal human bronchial epithelial (NHBE) cell 3D cultures for in vitro lung model studies. Sci. Rep. 9, 500.

Rubio, V., Valverde, M., Rojas, E., 2010. Effects of atmospheric pollutants on the Nrf2 survival pathway. Environ. Sci. Pollut. Res. 17, 369–382.

Rubio, V., Zhang, J., Valverde, M., Rojas, E., Shi, Z.-Z., 2011. Essential role of Nrf2 in protection against hydroquinone- and benzoquinone-induced cytotoxicity. Toxicol. In Vitro 25, 521–529.

Schmid, O., Cassee, F.R., 2017. On the pivotal role of dose for particle toxicology and risk assessment: exposure is a poor surrogate for delivered dose. Part. Fibre Toxicol. 14, 52.

Schmid, O., Möller, W., Semmler-Behnke, M., Ferron, G.A., Karg, E., Lipka, J., et al., 2009. Dosimetry and toxicology of inhaled ultrafine particles. Biomarkers 14, 67–73.

Schraufnagel, D.E., 2020. The health effects of ultrafine particles. Exp. Mol. Med. 52, 311–317.

Schwarze, P.E., Øvrevik, J., Hetland, R.B., Becher, R., Cassee, F.R., Låg, M., et al., 2007. Importance of size and composition of particles for effects on cells in vitro. Inhal. Toxicol. 19, 17–22.

Sillanpää, M., Geller, M.D., Phuleria, H.C., Sioutas, C., 2008. High collection efficiency electrostatic precipitator for in vitro cell exposure to concentrated ambient particulate matter (PM). J. Aerosol Sci. 39, 335–347.

Sotty, J., Garçon, G., Denayer, F.-O., Alleman, L.-Y., Saleh, Y., Perdrix, E., et al., 2019. Toxicological effects of ambient fine (PM2.5-0.18) and ultrafine (PM0.18) particles in healthy and diseased 3D organo-typic mucocilary-phenotype models. Environ. Res. 176, 108538.

Stewart, C.E., Torr, E.E., Mohd Jamili, N.H., Bosquillon, C., Sayers, I., 2012. Evaluation of differentiated human bronchial epithelial cell culture systems for asthma research. J. Allergy. 2012, 1-12.

Tyler, C.R., Zychowski, K.E., Sanchez, B.N., Rivero, V., Lucas, S., Herbert, G., et al., 2016. Surface area-dependence of gas-particle interactions influences pulmonary and neuroinflammatory outcomes. Part. Fibre Toxicol. 13, 64.

Zavala, J., Freedman, A.N., Szilagyi, J.T., Jaspers, I., Wambaugh, J.F., Higuchi, M., et al., 2020. New approach methods to evaluate health risks of air pollutants: Critical design considerations for in vitro exposure testing. Int. J. Environ. Res. Public. Health 17, 2124.

Zavala, J., Lichtveld, K., Ebersviller, S., Carson, J.L., Walters, G.W., Jaspers, I., et al., 2014. The gillings sampler – An electrostatic air sampler as an alternative method for aerosol in vitro exposure studies. Chem. Biol. Interact. 220, 158–168.

List of tables

Table 1. Flow rates for the operating conditions studied.

	CAST1	**CAST3**
Propane (mL/min)	60	60
Nitrogen (mL/min)	7	7
Oxidation air (L/min)	1.5	1
Dilution air (L/min)	20	20

Table 2. Geometric median (GM) mobility diameter, Count and Mass Concentration for each operating condition of the miniCAST.

Operating condition	**CAST1**	**CAST3**
GM (nm)	114 ± 1.54	58.9 ± 1.53
Count Concentration (N/cm^3)	6.12E+07	1,63E+08
Mass concentration (mg/m³)	89.4	57.9

Table 3. Mass deposition during exposures

Operating condition	**CAST1**	**CAST3**
Deposition efficiency (%)	0.29	1.3
Increase factor (+ 1000 V)	7.42	7.7
Mass deposition (ng/cm^2) in 35 min (0 V)	79.8	230.4
Mass deposition (ng/cm^2) in 35 min (+ 1000 V)	591.8	1775.0

List of figures

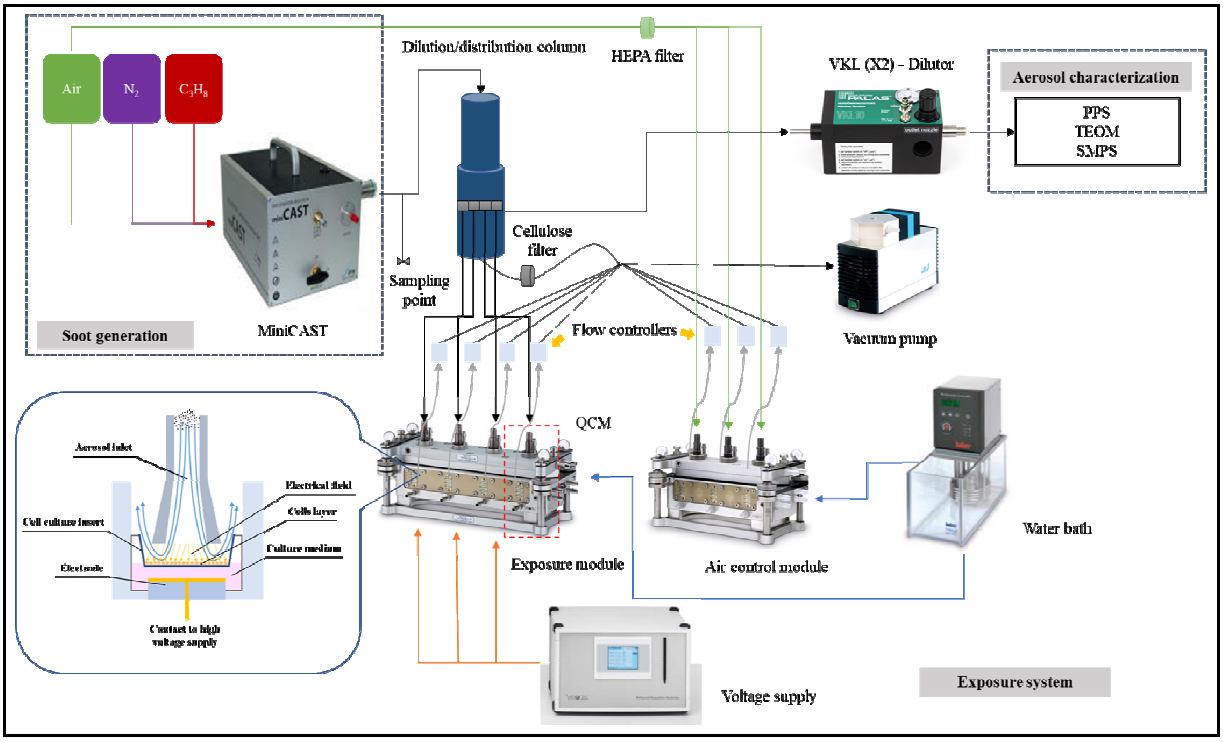

Fig. 1. Experimental setup.

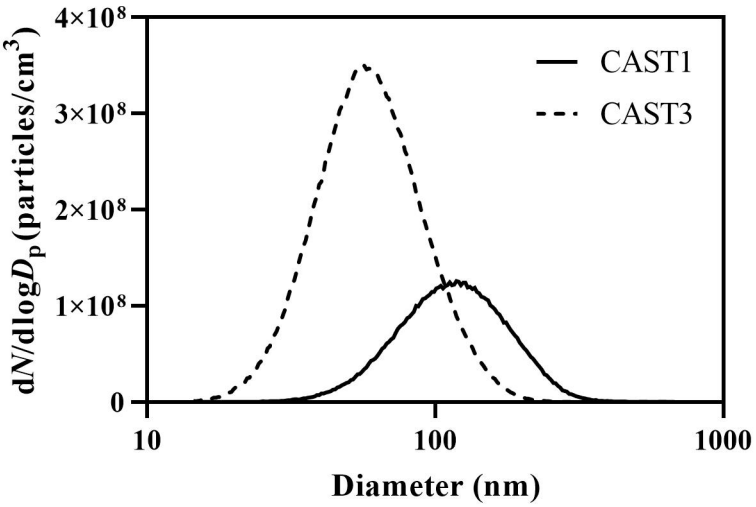

Fig. 2. Particle size distribution for each operating condition (corrected for VKL dilution).

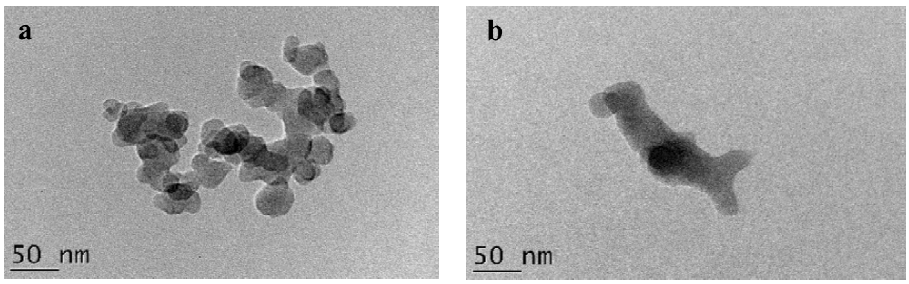

Fig. 3. Transmission electron microscopy images of particles generated at the two different operating conditions of the miniCAST (a: CAST1, b: CAST3).

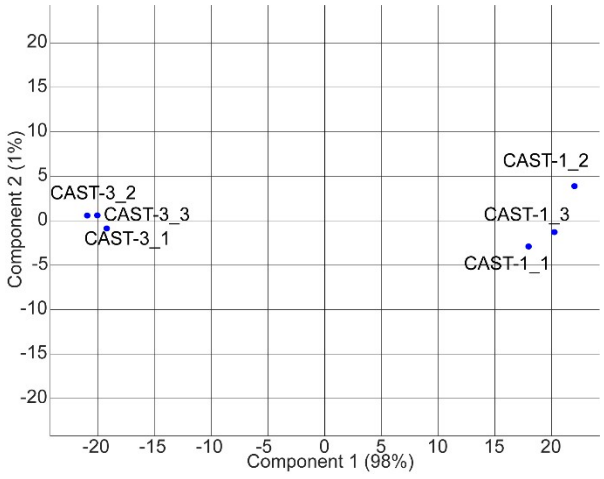

Fig. 4. Score plot from PCA visualizing the first two components (99% of variance).

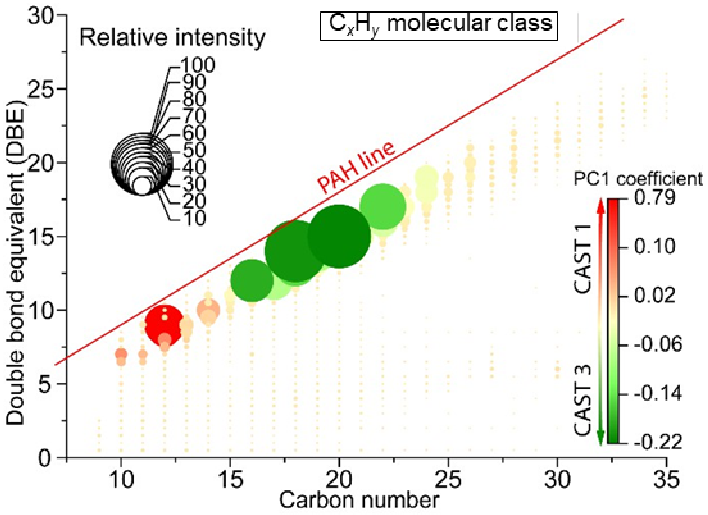

Fig. 5. Double-bond equivalent (DBE) vs carbon number plot of ions with molecular formulas containing only carbon and hydrogen (HC class). The dot size is indicative of the relative intensity of the ions and the colormap points to the PC1 loadings.

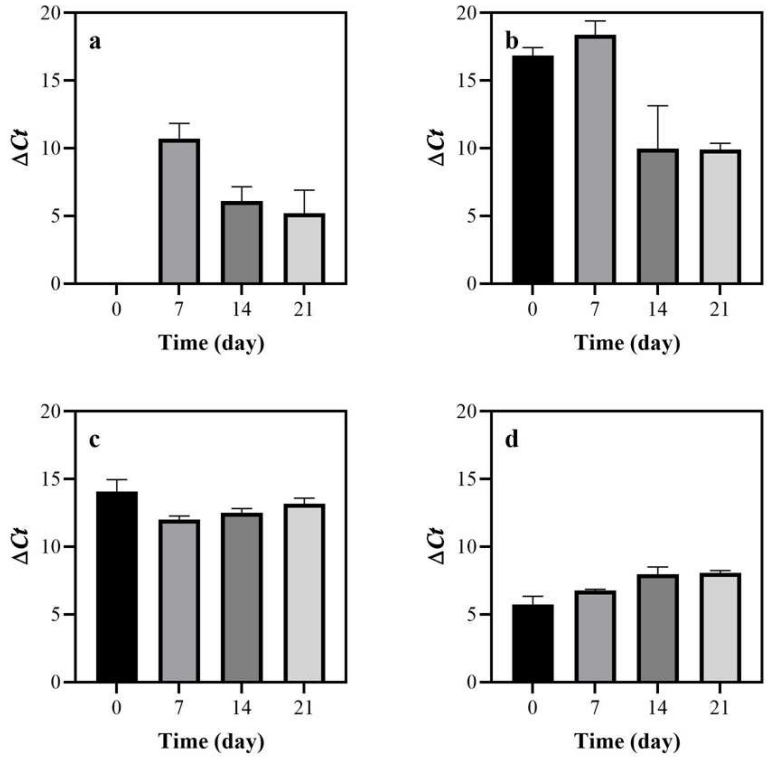

Fig. 6 mRNA expression of differentiation and tight junction markers. Primary cells were cultured at the ALI over 21 days. RNA was extracted at days 0, 7, 14 and 21 during ALI differentiation. Expression of (a) *MUC5AC,* (b) *FOX-J1*, (c) *OCLN* and (d) *ZO1*. Results are expressed as mean ± standard deviation (SD) of 2-3 independent experiments.

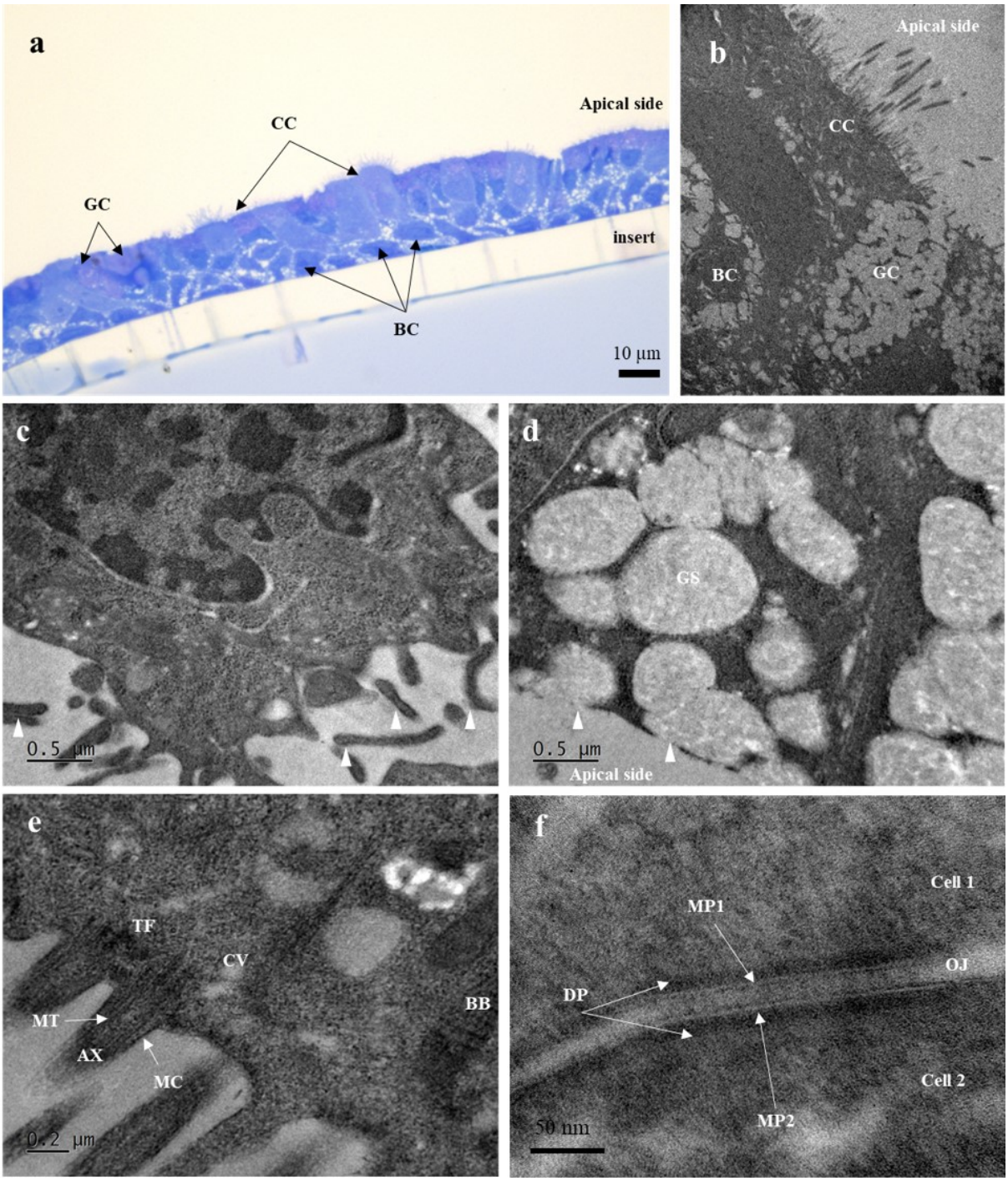

Fig. 7. Cellular structure and subcellular characterization of NHBE cells after 14 days of differentiation. (a) Optical microscopy of NHBE14-d. stained with metachromatic Toluidine blue. (b) Bright-field Transmission Electron Microscopy of NHBE, large field of view. (c) Basal cells with long cytoplasmic extensions (White arrowheads). (d) Goblet cells rich in mucus granules. Granules accumulate at the apical side of the cells to release their polysaccharide content in the extracellular space (White arrowheads). (e) Ciliated cells are well-differentiated as seen by the presence of mature motile cilia. (f) High-resolution TEM micrography of occludens junctions. Legend: GC: Goblet Cells; CC: Ciliated cells; BC: Basal

cell; GS: Secretory granules in goblet cells; BB: Basal body; AX: Axoneme; TF: Transition fiber; CV: Centriolar Vesicles; DP: Dense Plate; MP1: Plasma membrane cell 1; MP2: Plasma membrane cell 2.

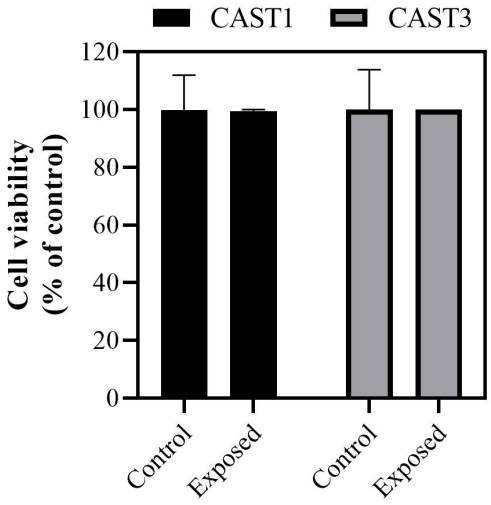

Fig. 8. Cell viability determined by MTT test 3 hr after exposure to CAST1 and CAST3 (+1000 V) aerosol. The data are expressed as mean ± SD of 3-4 independent experiments.

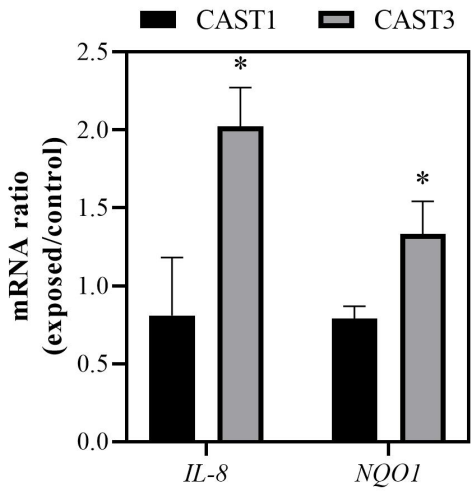

Fig. 9. Gene expression in NHBE cells exposed to particles. Cells were exposed to CAST1 and CAST3 particles (+1000 V) for 35 min and incubated with particles for 3 hr. Results are expressed as mean ± SD of 3-4 independent experiments. * Statistically significant differences are reported with $p < 0.05$.

JES-21-00494 Graphical abstract